these values are not unreasonable for normal reflected daytime illumination, some of the observational conditions under which the velocity illusion has been noted involved appreciably less illumination. If the extrapolation of laboratory measurements is valid, this implies a discrepancy for the increased velocity illusion (that is, when the covered eye is in a leading position). It may be, however, that the tiring of an observer experienced under apparently increased velocity and the occasional impression of confusion are reflections of some compensatory mechanism operative when apparent interocular distance would otherwise be negative; in this case, a 3-msec limit for the latency difference would not be a reliable determination.

Observations from a moving vehicle cannot, of course, readily provide quantitative data of the sort that can be easily obtained in a simplified laboratory situation with a swinging pendulum or oscillating target. Furthermore, the distortion of apparent distance, which is probably the "primary" illusion, seems to be entirely explicable as a constant-velocity corollary of the Pulfrich pendulum illusion. Nevertheless, there are several significant implications of the observed phenomena. The fact that the illusion from an automobile persists during prolonged exposure to uniform "target" velocity demonstrates both an independence of the effect from accelerations inherent in oscillatory motion and a general lack of accomodation. The "dwarfing" of objects of known size serves as a striking nonlaboratory demonstration of how compelling stereopsis can be as a determinant of distance perception, in the face of conflicting supplementary information. Furthermore, the distortions of subjective velocity, which seem entirely "reasonable" in a moving field in which distance is wrongly evaluated, provide evidence for the importance of stereoptic evaluations of distance as a factor in motion perception (*3*).

J. T. ENRIGHT
Scripps Institution of Oceanography, University of California, La Jolla

References and Notes

1. C. Pulfrich, *Naturwissenschaften* **10**, 553, 569, 596, 714, 735, 751 (1922). Pulfrich himself (as have many others since) experimented not with a pendulum but with a peg oscillating on a linear pathway with sinusoidal changes in velocity.
2. R. H. Kahn, *Pfluegers Arch. Gesamte Physiol. Menschen Tiere* **228**, 213 (1931).
3. K. N. Ogle, in *The Eye*, H. Davson, Ed. (Academic Press, New York, 1962), vol. 4, p. 271.
4. M. H. Fischer and W. Mex, *Pfluegers Arch. Gesamte Physiol. Menschen Tiere* **252**, 478 (1950).
5. H. J. Engel and M. H. Fischer, *ibid.* **253**, 1 (1950).
6. M. Monjé, *ibid.* **249**, 280 (1947); A. Lit, *Amer. J. Psychol.* **62**, 159 (1949).
7. G. S. Wilson, *Brit. J. Physiol. Opt.* **22**, 208 (1965); E. Engelking and F. Poos, *Arch. Opthalmol.* **114**, 340 (1924); W. Best, *Pfluegers Arch. Gesamte Physiol. Menschen Tiere* **251**, 167 (1949); M. H. Fischer and I. Kaiser, *ibid.* **252**, 331 (1950); A. Lit. and A. Hyman, *Amer. J. Optom.* **28**, 564 (1951); R. H. Dittler, U. Roseman, H. H. Buchmann, *Z. Biol.* **105**, 40 (1952); M. H. Fischer, *ibid.*, p. 66; D. Trincker, *Pfluegers Arch. Gesamte Physiol. Menschen Tiere* **257**, 290 (1953); M. S. Katz and I. Schwartz, *J. Opt. Soc. Amer.* **45**, 523 (1955); R. Efon, *Brain* **86**, 295 (1963). These publications, together with references (*1–6*), provide a representative but by no means exhaustive coverage of the literature.
8. Full credit for noticing this illusion and bringing it to my attention goes to my son, Phillip N. Enright.
9. R. H. Kahn [*Pfluegers Arch. Gesamte Physiol. Menschen Tiere* **228**, 213 (1931)] reports, however, that, with considerable concentration and fixation on the oscillating pendulum bob, he was able subjectively to force the pendulum back into a planar oscillation, with the result that the rest of the room underwent startling oscillations in space.
10. Velocity, 80 km/hr = 22.2 mm/msec; a typical adult interocular distance is of the order of 60 to 65 mm.
11. This extrapolation is based on the data of Monjé [*Pfluegers Arch. Gesamte Physiol. Menschen Tiere* **249**, 280 (1947)] on the assumptions that latency difference at high intensities continues to be linearly related to the logarithm of the intensity and, on the basis of Lit's data [*Amer. J. Psychol.* **62**, 159 (1949)], that the slope of the relationship is proportional to the logarithm of the ratio of the intensity in the uncovered eye to that in the covered eye.
12. Supported by NSF grant GB 5471. I thank H. W. Honegger for helpful discussion of these results.

23 January 1970; revised 9 March 1970

Mercury: Surface Features Observed during Radar Studies

Abstract. *Radar studies of Mercury have shown the presence of several large, rough surface features and of one smooth area.*

Several large topographic features have been observed on Mercury during recent radar scans of that planet. The features appear to be almost continent-sized and are fixed to the surface and rotate with the planet. They have the ability to depolarize microwaves (12.5-cm wavelength) more strongly than neighboring areas do and are presumably rougher, to the scale of the wavelength.

The radar observations were made at the Jet Propulsion Laboratory's Goldstone tracking station in the Mojave Desert. Mercury is a very difficult target, having about the radar effectiveness of a dime at 16,000 km. The Goldstone radar facility, however, has tremendous capability which is summarized as follows: average power, 450 kw; wavelength, 12.5 cm; antenna gain (two-way), 4×10^{11}; and system noise temperature, 25°K.

Circularly polarized, monochromatic waves were beamed at Mercury. The weak returning echoes were no longer monochromatic. They were spectrally broadened by the Doppler effect which is caused by the rotation of Mercury. The actual data are in the form of spectrograms of the echoes, averaged over several hours to reduce the fluctuations of the noise.

Altogether, a dozen spectrograms were taken during the interval from 24 May to 13 June 1969. Half the data were taken with the receiver set for the expected sense of polarization of the echoes. These spectrograms show that much of the echoes originate from the quasi-specular region surrounding the sub-earth point.

The balance of the data was taken with the receiver set for the opposite sense of circular polarization, the so-called depolarized mode. The resulting spectrograms, weaker in power by a factor of 11, show topographic features

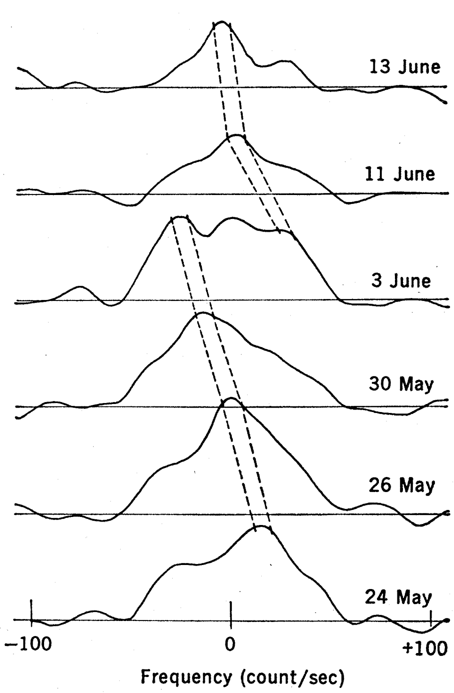

Fig. 1. Spectrograms of depolarized radar echoes from Mercury taken on six separate days. Power density is plotted against Doppler frequency shift. Spectral salients, corresponding to surface features on Mercury, are indicated by dashed lines.

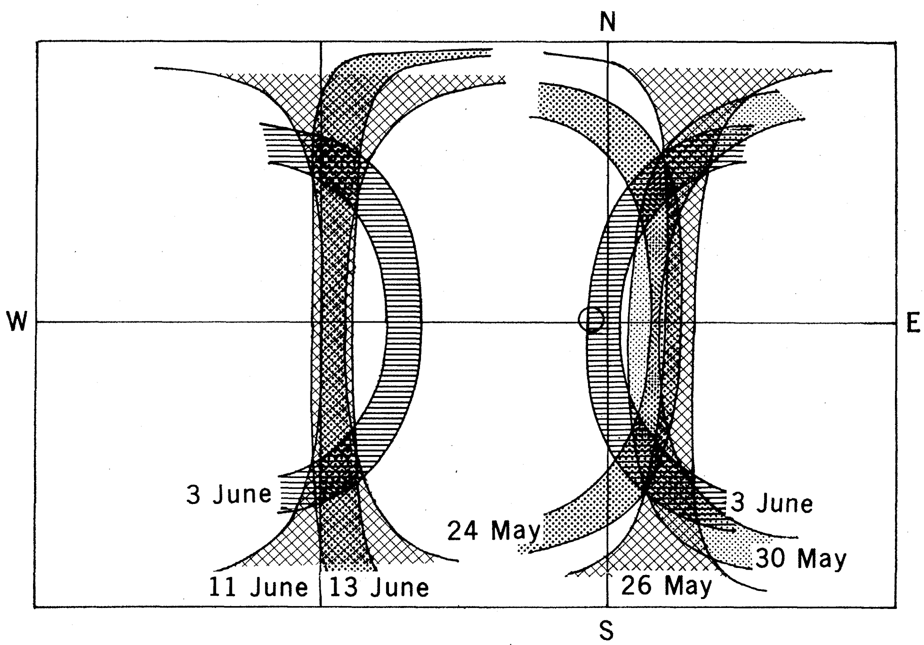

Fig. 2. Latitude-longitude coordinate frame for Mercury, with a grid spacing of 90°. The central meridian was arbitrarily chosen to include the sub-earth point on 30 May 1969. Each band marks possible locations for a surface feature required to cause a spectral salient. The surface feature must lie on band intersections.

of Mercury. These spectrograms are reproduced in Fig. 1.

The features reveal themselves as salients that move across the spectrograms, from the high-frequency side to the low, carried by Mercury's rotation. Two such trajectories are shown as dashed lines in Fig. 1. Although knowledge of the Doppler frequency of a feature is not sufficient to permit one to locate it uniquely on the planet, the Doppler frequency does define a locus of points that must include the feature.

Figure 2 is a latitude-longitude coordinate frame for Mercury. Each band marked out on Fig. 2 corresponds to a spectral salient of Fig. 1. The center of reflection of each feature must lie where the bands intersect. The fact that the several bands intersect demonstrates that the spectral salients do indeed correspond to features on Mercury. The fact that the intersections are not perfect shows that the long hours of signal averaging have not removed all of the system noise.

The band intersections have occurred in two places for each feature, one north of the equator and one south. It is not possible to distinguish which is the correct hemisphere from the data we have. If these objects were to be examined from a different point of view, however, the ambiguity could be resolved easily.

A third feature can be seen in the central spectral salient of 3 June. Unfortunately, there was an 8-day hiatus in the availability of the antenna for radar experiments, and that feature rotated out of view before Mercury could again be examined.

It was necessary to know the magnitude and direction of Mercury's spin vector before the computations of Fig. 2 could be made. The period of Mercury's rotation had long been thought to equal the orbital period of 88 days. However, radar observations by Pettengill and Dyce (*1*) in 1965 showed that the period was close to 59 days.

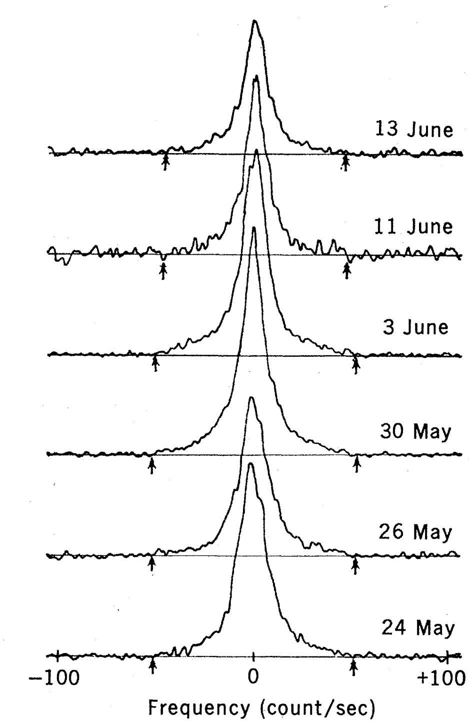

Fig. 3. Spectrograms of directly polarized echoes from Mercury. Arrows indicate theoretical spectral limits.

Theoretical investigations, by Columbo and Shapiro (*2*) and by Peale (*3*), stimulated by the radar data, showed that the rotational period of Mercury is likely to be locked at two-thirds of the orbital period. Furthermore, the spin axis could be expected to be perpendicular to the orbital plane either of Mercury or of the "average" of the other planets. The exact case would depend on the internal structure of Mercury.

I presumed a rotational period for Mercury that is two-thirds of the orbital period in the computations of Fig. 2. To check this, I computed the maximum and minimum Doppler shifts for each day and compared these values with the spectrograms taken in the polarized mode. These spectrograms are reproduced in Fig. 3, where the computed Doppler extremes are marked by arrows. As can be seen, the general agreement with the spectral edges is excellent. I also tested both of the likely orientations of the axis and found that the difference was imperceptible in the band structures of Fig. 2.

Although the spectrograms of Fig. 3 have an order of magnitude more power than the depolarized radar echoes, they show little indication of the presence of features. With one exception, they are all similarly shaped, having a blunt-nosed, high central peak. The spectrogram of 30 May, however, has a much sharper central peak than the others. This indicates that on that day a much smoother area was at the sub-earth point. The location of this smooth feature is marked with a circle on Fig. 2.

The rough features of Mercury seem similar to the ones we have earlier observed on Venus. They are larger, relative to the size of the disk, and have much less contrast with the surrounding areas. Part of this reduction in contrast can be attributed to the generally smoother surface of Venus. The rough features of both Mercury and Venus seem to share an affinity for middle latitudes.

R. M. GOLDSTEIN

Jet Propulsion Laboratory, California Institute of Technology, Pasadena 91103

References and Notes

1. G. H. Pettengill and R. B. Dyce, *Nature* **206**, 1240 (1965).
2. G. Columbo and I. I. Shapiro, *Astrophys. J.* **145**, 296 (1966).
3. S. J. Peale, *Astron. J.* **74** (3), 483 (1969).
4. This report presents the results of one phase of research carried out at the Jet Propulsion Laboratory, California Institute of Technology, under NASA contract No. NAS 7-100.

23 January 1970

Superheated Ice Formed by the Freezing of Superheated Water

Abstract. *Water, superheated with respect to the vapor phase, has been made to freeze, thus forming ice that is also superheated with respect to the vapor. This phase transformation occurred at the extension of the melting curve below the triple point pressure.*

The possibility that a superheated liquid could undergo a phase change to form a superheated solid has been suggested by Pippard (*1*). We have succeeded in demonstrating that this phase transformation between metastable states can indeed take place.

In order to understand this phenomenon let us consider a simple substance which exhibits the three phases solid, liquid, and vapor, characterized by the thermodynamic variables pressure p, temperature T, and the Gibbs function per unit mass g. The phase diagram for the stable or equilibrium states of the substance (Fig. 1a) is the projection of the intersections of the surfaces of minimum g. These intersections define three lines: *S-L*, *L-V*, and *V-S* at which transitions between the stable phases occur. These lines, which correspond to the melting, evaporation, and sublimation curves, respectively, intersect at the triple point.

The fact that metastable states of a substance exist makes it appropriate to continue the g-surface for each phase beyond those values of p and T delineated by the equilibrium phase diagram. Thus phase diagrams for the metastable states (Fig. 1, b and c) may be constructed from the projections of the intersections of the surfaces having intermediate and maximum values of g, denoted by subscripts I and II, respectively (*2*). These metastable phase diagrams suggest that phase transitions between metastable states and "stability transitions" between stable and metastable states of the same phase could, in principle, occur. A summary of both known and hypothetical phase and stability transitions is given in Table 1. In the experiment reported here, we describe the first observations of the phase transitions: (i) $L_{II} \rightarrow S_I$, the formation of a superheated solid by the freezing of a superheated liquid; (ii) either $S_I \rightarrow V$ or $S_I \rightarrow V_I$, the sublimation of a superheated solid to produce either a stable or a supercooled vapor; and (iii) the stability transition $L_I \rightarrow L_{II}$, the supercooling of superheated liquid at pressures below the triple point.

When the chamber pressure of a vacuum chamber containing a beaker of water falls to the vapor pressure of the water, as determined by its temperature, the water will begin to boil and then to cool, and the system will follow the vapor pressure curve as the pressure is reduced further. At the triple point pressure, a layer of ice will rapidly form at the water surface. However, the behavior of water subjected to such diminishing pressure will be quite different if the water has no free surface. In the experiment reported here the free surface of the water was removed by covering the water with a layer of triethylbenzene $C_6H_3(C_2H_5)_3$. This clear, colorless liquid is insoluble in water and has a specific gravity of 0.87 and a low vapor pressure.

The experimental apparatus is sketched in Fig. 2. The thermocouple (accurate to within 0.1°C) was located just below the triethylbenzene-water interface. Special care was taken to ensure that the thermocouple did not make contact with the beaker walls in the water, as such contacts serve as nucleation points for violent boiling which would prevent reduction of the pressure to less than that of the triple point. The weight per unit area of the triethylbenzene layer is 0.64 mm-Hg and the weight per unit area of a layer of H_2O 2.5 cm thick is 1.84 mm-Hg. At the bottom of the water the pressure is the sum of the chamber pressure and 2.48 mm-Hg. The entire apparatus was placed in a vacuum glass bell jar 45.5 by 76 cm with the oil bath resting on a plate cooled by liquid nitrogen. The heat capacity of the oil bath prevents the water from experiencing sudden changes in its thermal environment.

Before the water was covered with the triethylbenzene, it was thoroughly degassed. The degassing was accomplished by placing the water in the vacuum chamber and slowly reducing the pressure until ice formed on the water surface. After the ice had been removed and the water had been covered with degassed triethylbenzene (the oil was also degassed by exposure to

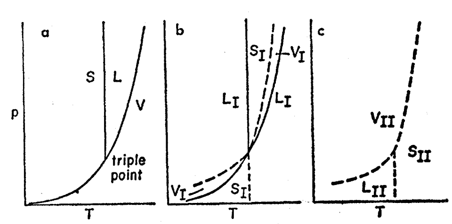

Fig. 1. Phase diagrams for a simple substance exhibiting the three phases solid, liquid, and vapor. (a) Equilibrium phase diagram. (b) Projection of intersections of surfaces having intermediate values of g, that is, the phase diagram for the first metastable state. (c) Projection of intersections of surfaces having maximum g-values, that is, the phase diagram for the second metastable state.

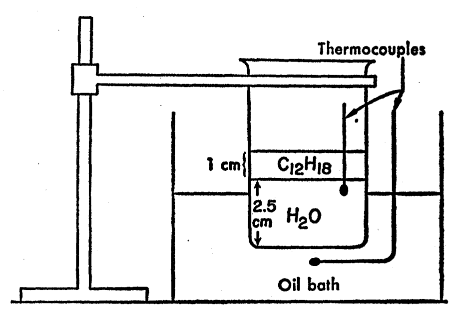

Fig. 2. Schematic of the experimental apparatus.

Table 1. Possible phase and stability transitions for a substance exhibiting the three phases solid, liquid, and vapor.

Type of transition	*S-L* line	*L-V* line	*V-S* line
	Pressures above the triple point pressure		
Phase	$S \rightleftharpoons L$, $S \rightleftharpoons L_I$,	$L \rightleftharpoons V$, $L \rightleftharpoons V_I$,	$S_I \rightleftharpoons V_I$, $S_I \rightleftharpoons V_{II}$,
Phase	$S_I \rightleftharpoons L$, $S_I \rightleftharpoons L_I$	$L_I \rightleftharpoons V$, $L_I \rightleftharpoons V_I$	$S_{II} \rightleftharpoons V_I$, $S_{II} \rightleftharpoons V_{II}$
Stability	$S \rightleftharpoons S_I$, $L \rightleftharpoons L_I$	$L \rightleftharpoons L_I$, $V \rightleftharpoons V_I$	$S_I \rightleftharpoons S_{II}$, $V_I \rightleftharpoons V_{II}$
	Pressures below the triple point pressure		
Phase	$S_I \rightleftharpoons L_I$, $S_I \rightleftharpoons L_{II}$,	$L_I \rightleftharpoons V_I$, $L_I \rightleftharpoons V_{II}$,	$V \rightleftharpoons S$, $V \rightleftharpoons S_I$,
Phase	$S_{II} \rightleftharpoons L_I$, $S_{II} \rightleftharpoons L_{II}$	$L_{II} \rightleftharpoons V_I$, $L_{II} \rightleftharpoons V_{II}$	$V_I \rightleftharpoons S$, $V_I \rightleftharpoons S_I$
Stability	$S_I \rightleftharpoons S_{II}$, $L_I \rightleftharpoons L_{II}$	$L_I \rightleftharpoons L_{II}$, $V_I \rightleftharpoons V_{II}$	$V \rightleftharpoons V_I$, $S \rightleftharpoons S_I$